ARTICLE NO. 80-4048

Theoretical Investigation of the Aerodynamics of Double Membrane Sailwing Airfoil Sections

H. Murai* and S. Maruyama†
Tōhoku University, Sendai, Japan

The sailwing has many special characteristics due to its flexible structure. In order to estimate the sailwing performance theoretically, a numerical analysis method is presented for obtaining aerodynamic characteristics and profile forms of a sailwing with a rounded leading edge and upper and lower individual surface shapes. The trailing edge is fixed and membranes are not stretched by tension although they have slackness. Through numerical examples, it is shown that a sailwing of this type has a completely different pressure distribution from that of a single membrane sailwing with a leading edge of the circular cylinder or oval type. The latter has shape peaks in the pressure distribution which may have undesirable effects on the sailwing performance. These peaks in the pressure distribution can be removed by adopting a D-spar leading edge of some kind.

Nomenclature

c = chord length
C_L = lift coefficient
C_p = pressure coefficient $= (P-P_\infty)/\frac{1}{2}\rho U_\infty^2$
ΔC_p = pressure difference coefficient $= (P-P_i)/\frac{1}{2}\rho U_\infty^2$
C_{p_i} = internal pressure coefficient $= (P_i-P_\infty)/\frac{1}{2}\rho U_\infty^2$
C_T = nondimensional tension $= T/\frac{1}{2}\rho U_\infty^2 c$
l = length of membrane between the leading edge ($\xi=0$) and the trailing edge ($\xi=1$) (one side)
P, P_∞ = static pressure on wing surface, in freestream
P_i = internal pressure of sailwing
T = chordwise tension per unit span
U_∞ = freestream velocity
α = angle of attack
γ = nondimensional strength of vorticity
ϵ = $(l/c)-1$: nondimensional excess length of membrane
ξ, η = nondimensional coordinates x/c, y/c
ρ = density
ϕ = velocity potential
ψ_0 = stream function on airfoil surface (= constant)

Subscripts

i,j = ith, jth elements of the airfoil
L = leading edge spar coordinate
m = membrane coordinate
s = separation point of leading edge spar and membrane
u,l = upper surface, lower surface

Introduction

THE sailwing geometry dealt with in this report is shown in Fig. 1. It consists of a rigid leading edge spar (a), a tip rib and a root rib (b,c) which are fixed to the leading edge spar, a trailing edge wire (d) which is stretched between the tip and root ribs, and flexible wing surfaces (e,f) wrapped around the leading edge spar and the trailing edge, forming the upper and lower wing surfaces. The wing surfaces and the overall structure of the sailwing deform easily, and the aerodynamic characteristics of this type of a wing are very different from those of a rigid wing. The sailwing is expected to have various field applications.

Previous theoretical investigations of a sailwing through the linearized two-dimensional analyses by Thwaites,[1] Nielsen,[2] and Tuck, et al.,[3] as well as the application by Ormiston[4] of Nielsen's theory to a sailwing considering elongations of the membrane and the trailing edge wire, were all concerned with a sailwing consisting of a zero thickness single membrane. There are numerous experimental investigations of the aerodynamic characteristics of a sailwing[4-7] and of its application to the foldable light airplane[5,6] or to the windmill generator.[8,9] However, no theoretical investigation can be found of a sailwing which consists of a rounded leading edge and separate upper and lower wing surfaces, as shown in Fig. 1, although such a design is expected to have many aerodynamic and structural advantages, e.g., controllability by using internal pressure.

The present report presents a numerical analysis of the aerodynamic characteristics of such a sailwing, and shows the effect of leading edge shape and slackness (ϵ) on the pressure distribution through numerical examples.

Basic Equations

The following assumptions are made for simplicity in the analysis of a streamwise cross-section of the sailwing (Fig. 2).

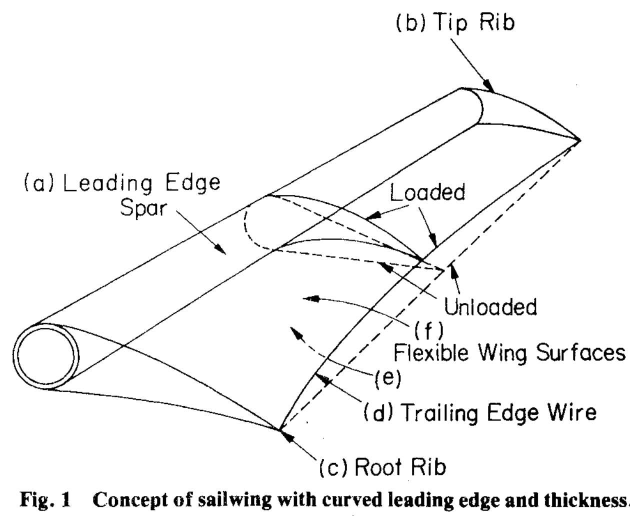

Fig. 1 Concept of sailwing with curved leading edge and thickness.

Received Oct. 18, 1978; revision received Aug. 22, 1979.

Index categories: Aerodynamics; Wind Power; Computational Methods.

*Professor, Institute of High Speed Mechanics.
†Postgraduate Student, Department of Mechanical Engineering.

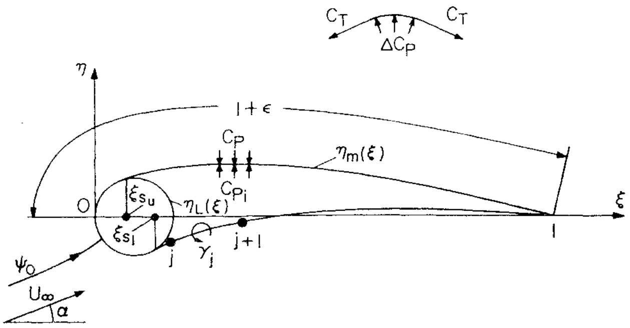

Fig. 2 Schematic model of sailwing cross-section.

1) Flow across the section is two-dimensional, inviscid, and incompressible.
2) The membrane has no porosity.
3) The membrane is flexible and has excess length $(c\epsilon)$, but does not stretch by tension.
4) The upper and lower membranes are fixed at the leading edge $[(\xi,\eta)=(0,0)$ in Fig. 2)$]$.
5) The coordinates of the leading edge spar and the trailing edge are fixed. This means that the deflection of the trailing edge wire is neglected.

As shown in Fig. 2, the coordinate of each surface is presented as follows:

$$\left.\begin{array}{ll}\eta(\xi)=\eta_L(\xi) & 0\leq\xi\leq\xi_s \\ \eta(\xi)=\eta_m(\xi) & \xi_s<\xi\leq 1\end{array}\right\} \tag{1}$$

The relation between the tension C_T (Fig. 2) and the difference in internal and external pressure ΔC_p is expressed as follows:

$$C_T\frac{(\mathrm{d}^2\eta/\mathrm{d}\xi^2)}{\{1+(\mathrm{d}\eta/\mathrm{d}\xi)^2\}^{3/2}}=\pm\Delta C_p \tag{2}$$

Equation (2) is valid generally. It expresses the force balance between the pressure difference (right-hand side) and the tension of a membrane (left-hand side) with the profile form $\eta=f(\zeta_0)$. In a practical sailwing, where the membrane slope $(\mathrm{d}\eta/\mathrm{d}\zeta)$ is small, Eq. (2) is reduced to the following simpler form

$$C_T\frac{\mathrm{d}^2\eta}{\mathrm{d}\xi^2}=\mp\Delta C_p \tag{3}$$

where C_T becomes the chordwise tension, − indicates the upper surface, and + the lower surface.

The boundary conditions of Eq. (3) are that the membrane and the leading edge spar separate smoothly at the point, $\xi=\xi_s$ which generally is different for the upper and lower surfaces:

$$\eta_m=\eta_L \tag{4}$$

$$\frac{\mathrm{d}\eta_L}{\mathrm{d}\xi}=\frac{\mathrm{d}\eta_m}{\mathrm{d}\xi} \tag{5}$$

The condition under which the trailing edge is fixed is:

$$\eta=0 \quad \text{at} \quad \xi=1 \tag{6}$$

By assuming that the membrane length $c(1+\epsilon)$ is constant, the nondimensional membrane length c is obtained as follows:

$$\int_0^{\xi_s}\sqrt{(\mathrm{d}\eta)^2+(d\xi)^2}+\int_{\xi_s}^{1}\sqrt{1+\left(\frac{\mathrm{d}\eta}{\mathrm{d}\xi}\right)^2}\mathrm{d}\xi=1+\epsilon \tag{7}$$

Equations (1-7) are satisfied independently for both the upper and lower surfaces. The resulting boundary value problem is to solve Eqs. (8) and (9) under the boundary conditions represented by Eqs. (3-7).

$$\frac{\partial^2\phi}{\partial\xi^2}+\frac{\partial^2\phi}{\partial\eta^2}=0 \tag{8}$$

$$\Delta C_p=C_{p_i}-C_p=C_{p_i}-1+\left\{\left(\frac{\partial\phi}{\partial\xi}\right)^2+\left(\frac{\partial\phi}{\partial\eta}\right)^2\right\} \tag{9}$$

Numerical Analysis

In order to solve the above boundary value problem, calculations of the effect of the pressure distribution on the sailwing surface deformation and the calculation of the potential flow around the deformed airfoil are carried out separately. The final solution is obtained by iteration of both calculations. By adopting the iteration method very accurate computation of the pressure distribution and profile shape is possible, even in the case of a highly cambered sailwing with a large leading edge radius. By referring to previous results for other similarly shaped sailwings, the first approximation of pressure distribution is made. The final solution can usually be obtained in a few iterations by this approximation.

Calculation of Airfoil Deformation

When ΔC_p is given, $\eta(\xi)$ can be obtained by integrating Eq. (3) as follows:

$$C_T\eta(\xi)=\mp\int_{\xi_s}^{\xi}\int_{\xi_s}^{\xi}\Delta C_p\mathrm{d}\xi\mathrm{d}\xi+C_1\xi+C_2 \tag{10}$$

where C_1 and C_2 are constants. In Eq. (10), the unknowns are ξ_s, C_T, C_1 and C_2, so that Eq. (10) must be solved by boundary conditions of Eqs. (4-7). However, the boundary condition equations (4, 5, 7) involve ξ_s, and ξ_s is also a limit of integration in Eq. (10). As Eq. (10) cannot be solved directly ξ_s is assumed to be at a selected point on the leading edge spar. A corresponding value $\eta=\eta'$ is calculated by using Eqs. (4-6, 10). By substituting η' in the left-hand side of Eq. (7), it is evaluated as follows:

$$\int_0^{\xi_s}\sqrt{(\mathrm{d}\eta')^2+(\mathrm{d}\xi)^2}+\int_{\xi_s}^{1}\sqrt{1+\left(\frac{\mathrm{d}\eta'^2}{\mathrm{d}\xi}\right)}\mathrm{d}\xi=1+\epsilon+\Delta\epsilon \tag{11}$$

where $\Delta\epsilon$ is the difference from the given ϵ, because the assumed separation point ξ_s is not correct. For the correct ξ_s value $\Delta\epsilon$ equals zero on the leading edge spar, and $\eta'(\xi)$ is the coordinate of the sailwing profile which fulfills all of the boundary conditions.

The accuracy of ϵ affects the pressure distribution and C_L, because ϵ greatly affects the camber of the airfoil. The practical calculation of ξ_s is divided into three stages in order to make $\Delta\epsilon$ sufficiently small or close to zero. The coordinate of the leading edge in each stage is determined by means of Lagrange's interpolation. Since the upper and lower surface calculations are conducted independently it might happen that the upper and lower surfaces cross near the trailing edge, which would be impossible in a real sailwing. However, this anomaly is made sufficiently small so that its effect on the pressure distribution near the trailing edge is no more than the effect of the thick boundary layer. Therefore, the computed upper and lower surfaces are attached at the trailing edge to the middle point of both calculated surfaces.

Calculation of Pressure Distribution

There are many calculation methods for the pressure distribution of a two-dimensional arbitrary airfoil. Of these, Oeller's method[10] and that of Hess, et al.,[11] have been combined and improved in order to make them suitable for the calculation of a sailwing which, as mentioned in the previous section, may attach the upper and lower surfaces near the trailing edge.

Considering the singularities at the leading and trailing edges the coordinates for the sailwing profile are divided as follows:

$$\xi_i = \frac{1}{2}(1+\cos\theta); \qquad \theta = \frac{2\pi(i-1)}{N}$$

$$i = 1,2,\ldots,N+1 \qquad (12)$$

By means of Oeller's method,[10] the vortex sheets are distributed on segments of the airfoil surface in order to satisfy the condition that the stream function ψ_0 is constant on the airfoil surface. Because the upper and lower surfaces may attach near the trailing edge, as mentioned above, these calculations are conducted separately for two cases:

1) The case where the upper and lower surface do not attach. In this case the method for calculating the vortex distribution is the same as Oeller's, that is, under Kutta's condition:

$$\gamma_1 = -\gamma_N \qquad (13)$$

$(N+1)$ simultaneous equations are calculated as follows:

$$\begin{bmatrix} K_{11} & \cdots & K_{1N} & 1 \\ \vdots & & \vdots & \vdots \\ K_{N1} & \cdots & K_{NN} & 1 \\ 1 & 0 \cdots 0 & 1 & 0 \end{bmatrix} \begin{bmatrix} \gamma_1 \\ \vdots \\ \gamma_N \\ \psi_0 \end{bmatrix} = \begin{bmatrix} B_1 \\ \vdots \\ B_N \\ 0 \end{bmatrix} \qquad (14)$$

$$K_{ij} = \frac{1}{2\pi}\left[\frac{1}{2}\{\xi'_{j+1}\ln(\xi'^2_{j+1}+\eta'^2_{j+1}) - \xi'_j\ln(\xi'^2_j+\eta'^2_j)\}\right.$$
$$\left. -\{\xi'_{j+1}-\xi'_j\} + \eta'_{j+1}\left\{\tan^{-1}\frac{\xi'_{j+1}}{\eta'_{j+1}} - \tan^{-1}\frac{\xi'_j}{\eta'_j}\right\}\right] \quad \text{for} \quad i \neq j$$
$$= \frac{1}{2\pi}\left\{\Delta S\left(\ln\frac{\Delta S}{2} - 1\right)\right\} \quad \text{for} \quad i=j$$

ΔS; length of jth element, (15)

$$B_i = \frac{(\eta_i+\eta_{i+1})}{2}\cos\alpha - \frac{(\xi_i+\xi_{i+1})}{2}\sin\alpha \qquad (16)$$

where ξ', η' are coordinates which have origin at the center of the ith element, and the direction of the ξ' axis is equal to one of the jth elements.

2) The case where both surfaces attach. When k elements of the upper and lower surfaces attach forward of the trailing edge, this portion is replaced by a set of single vortex sheets. Therefore, the number of vortex sheets is $(N-k)$. From Eq. (12), the first element is considered to be small enough when N is taken to be large. Kutta's condition is

$$\gamma_1 = 0 \qquad (17)$$

Then the equation of vortex sheets becomes $(N-k+1)$ simultaneous equations as follows:

$$\begin{bmatrix} K_{11} & \cdots & K_{1,N-k} & 1 \\ \vdots & & \vdots & \vdots \\ K_{N-k,1} & \cdots & K_{N-k,N-k} & 1 \\ 1 & 0 \quad 0 & 0 & 0 \end{bmatrix} \begin{bmatrix} \gamma_1 \\ \vdots \\ \gamma_{N-k} \\ \psi_0 \end{bmatrix} = \begin{bmatrix} B_1 \\ \vdots \\ B_{N-k} \\ 0 \end{bmatrix} \qquad (18)$$

When the distribution of vortex sheets is calculated, the tangential velocity components of each element, induced by the vortex of unit strength A_{ij} are presented as follows based upon the method of Hess, et al.[11]

$$A_{ij} = -V_x\sin\theta + V_y\cos\theta \qquad (19)$$

$$V_x = \frac{1}{4\pi}\ln\left[\frac{(X'+\Delta S/2)^2+y'^2}{(X'-\Delta S/2)^2+y'^2}\right] \quad \text{for} \quad i\neq j$$
$$=0 \quad \text{for} \quad i=j \qquad (20)$$

$$V_y = \frac{1}{2\pi}\left[\tan^{-1}\left(\frac{X'+\Delta S/2}{y'}\right) - \tan^{-1}\left(\frac{X'-\Delta S/2}{y'}\right)\right] \quad \text{for} \quad i\neq j$$
$$= -\frac{1}{2} \quad \text{for} \quad i=j \qquad (21)$$

where X', y' are the coordinates of the center of the ith element with their origin at the center of the jth element. The direction of the X'-axis is tangent to the ith element and θ is the angle between the X'-axis and the ith element. The velocity distribution on the airfoil is calculated as the sum of the induced tangential velocities and the uniform freestream velocity.

Comparison of Numerical Calculation with Exact Pressure Distribution and Analytical Solution

First, the pressure distributions calculated by the method mentioned in the above section are compared with exact solutions obtained by conformal transformation. Figs. 3a and 3b show the comparisons of pressure distributions for a flat plate and a thick cambered Joukowski airfoil, respectively. The numerical results are shown to be very close to the exact solutions.

Figures 4 and 5 show the $C_L(\alpha)$ and $C_T(\alpha)$ relations calculated by the present method and by Nielsen's analytical method[2] for the case of a single two-dimensional flexible aerodynamic surface of zero thickness. In this case, ΔC_p in Eq. (3) is the difference of C_p on the upper and lower surfaces. The boundary conditions are

$$\eta = 0 \quad \text{at} \quad \xi = 1,0 \qquad (22)$$

C_T is calculated as follows. By eliminating Eq. (7), because $(\mathrm{d}\eta/\mathrm{d}\xi)$ is small for a practical sailwing, one obtains

$$\epsilon = \int_0^1 \sqrt{1+\left(\frac{\mathrm{d}\eta}{\mathrm{d}\xi}\right)^2}\,\mathrm{d}\xi - 1 \doteqdot \frac{1}{2}\int_0^1 \left(\frac{\mathrm{d}\eta}{\mathrm{d}\xi}\right)^2 \mathrm{d}\xi \qquad (23)$$

As the right-hand side of Eq. (23) is given by the integration of Eq. (3), C_T can be deduced as follows:

$$C_T = \frac{1}{2\epsilon}\int_0^1 \left(-\int_0^\xi \Delta C_p \mathrm{d}\xi + C_1\right)^2 \mathrm{d}\xi \qquad (24)$$

where

$$C_1 = \int_0^1 \int_0^1 \Delta C_p \mathrm{d}\xi\mathrm{d}\xi$$

In the calculation of the pressure distribution the method given in the previous section for case 2 is adopted. Figures 4 and 5 show $C_L(\alpha)$ in the case of $\epsilon = 1$ and 4%, and $C_T(\alpha)$ in

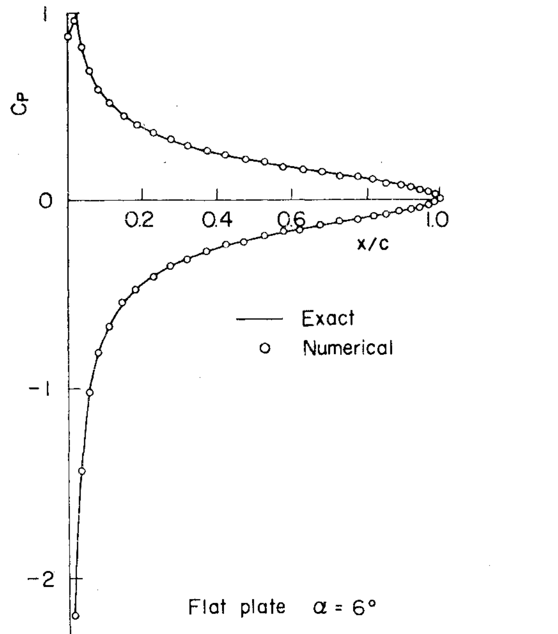

Fig. 3a Comparison of pressure distribution on flat plate with exact solution.

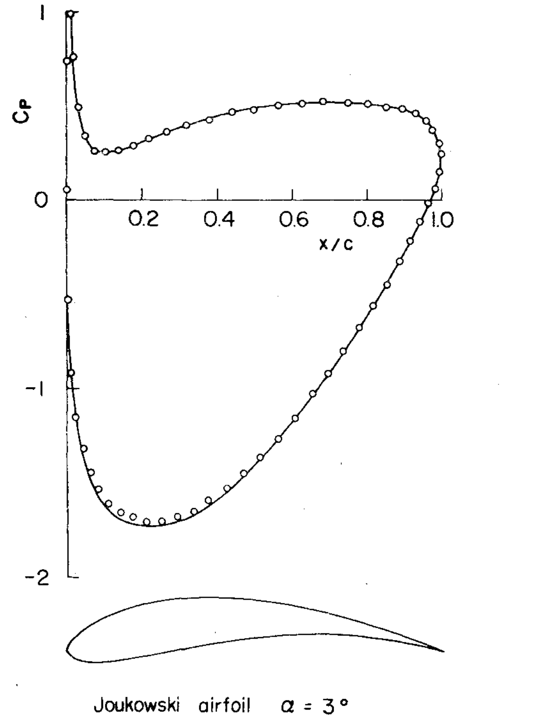

Fig. 3b Comparison of pressure distribution on Joukowski airfoil with exact solution.

the case of $\epsilon = 1\%$. For $\epsilon = 1\%$ the numerical results are in relatively good accordance with Nielsen's analytical solutions using Fourier series.[2] However, the $C_L(\alpha)$ relations in the case of $\epsilon = 4\%$ show some deviation between the two methods. This is considered to be due to the lack of validity of Nielsen's linearized theory as $\epsilon = 4\%$ produces a rather large camber.

Figures 4 and 5 show the results obtained using the first approximation of the pressure distribution in order to insure that the airfoil shape stays convex. Under this initial condition, the numerical results for C_T is larger than $C_T\alpha_{\min}$ are in good agreement with Nielsen's solutions in Fig. 5. Solutions for C_T's smaller than $C_T\alpha_{\min}$ cannot be obtained by

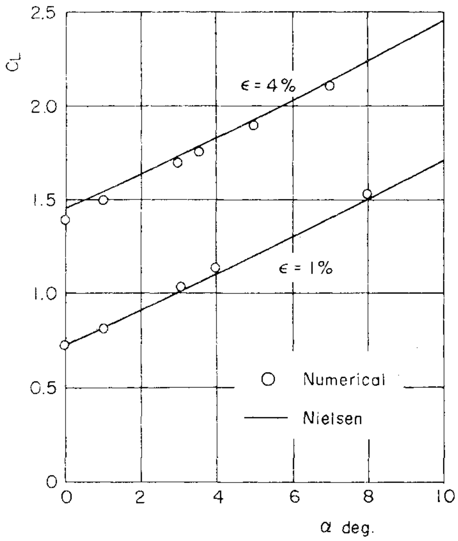

Fig. 4 Comparison of $C_L - \alpha$ relations with Nielsen's.

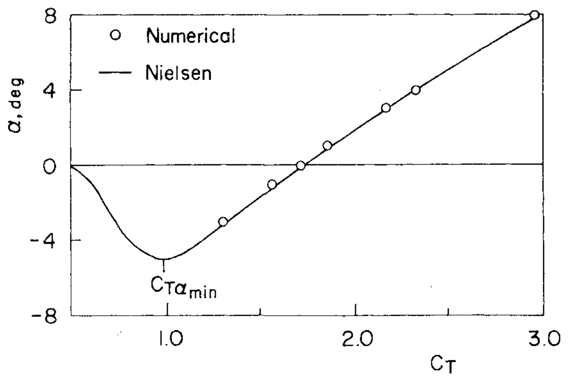

Fig. 5 Comparison of $\alpha - C_T$ relations with Nielsen's, when $\epsilon = 1\%$.

the present numerical analysis. This case is left for future improvement of the present analysis.

Calculation Results

Figures 6-10 show calculated results which represent the typical pressure distributions and profile forms of sailwings. In these figures, profile forms and pressure distributions are indicated for given α and ϵ. The associated calculated values for C_L and C_T are also shown. C_T is an essential parameter when the strength of the membrane is given for the design of sailwings. In these calculations, the first approximation of the pressure distribution is obtained prescribing convex upper and lower surfaces. The internal pressure P_i is set equal to P_∞, i.e. $Cp_i = 0$. The calculated results for single and double membranes sailwings are shown in Fig. 6. The two sailwings have the same α and almost the same C_L. However, the double membrane sailwing with rounded leading edge has a pressure distribution completely different from the one for the single membrane wing.

The pressure distribution in Fig. 7 show that the moment center of a sailwing with relatively large slackness is more rearward than that of a conventional rigid wing. In addition, large lift ($C_L = 1.65$) is obtained at a relatively low angle of attack. These characteristics are in accordance with Fink's experimental results.[7] When the membranes have smaller slackness (ϵ) the characteristics approach those of a conventional rigid wing, as can be seen in Fig. 8. The pressure distribution in Fig. 7 has sharp peaks of minimum pressure coefficient near the point where the membrane separates from the leading edge spar. These peaks cause boundary layer

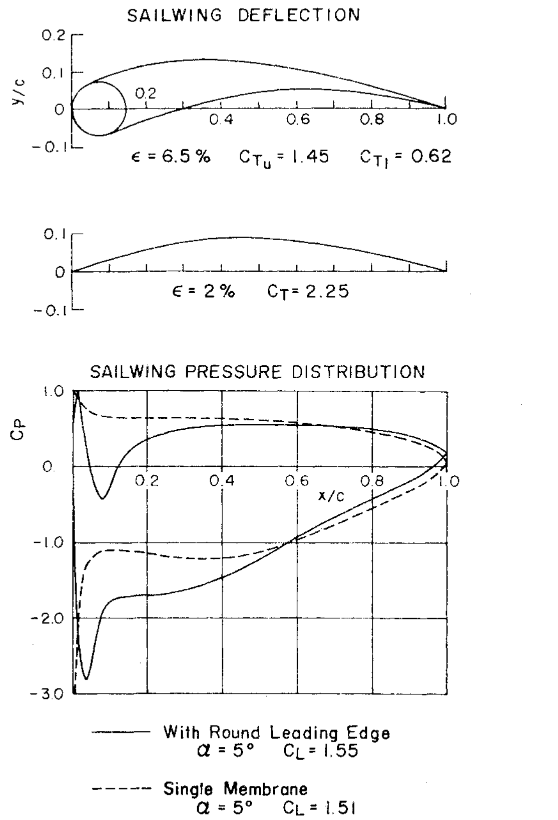

Fig. 6 Profile forms and pressure distributions of sailwing with round leading edge of 15% chord diameter and sailwing of no thickness at same angle of attack.

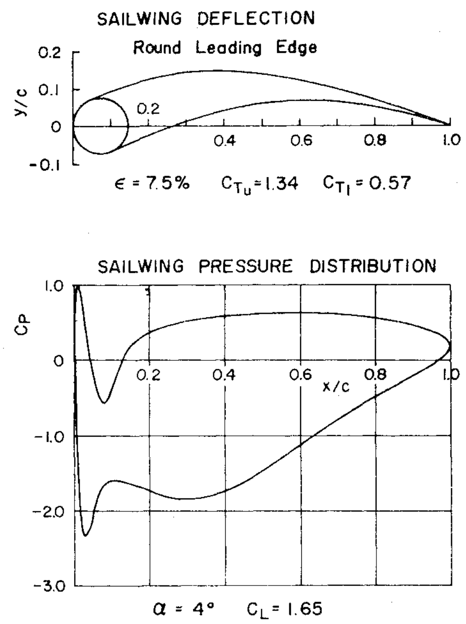

Fig. 7 Sailwing with round leading edge of 15% chord diameter.

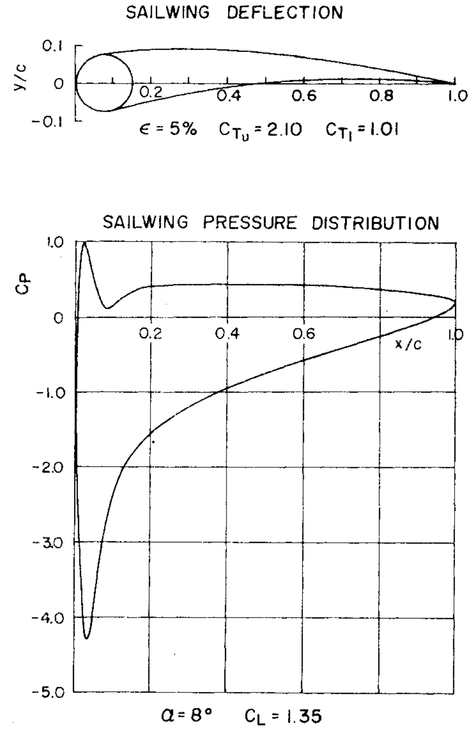

Fig. 8 Sailwing with round leading edge with small slackness.

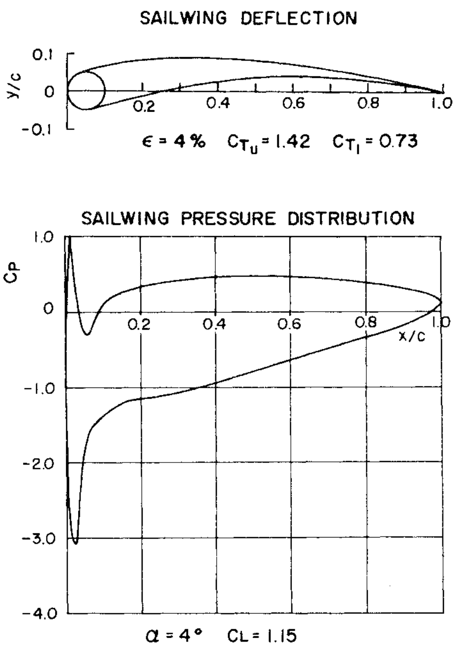

Fig. 9 Sailwing with round leading edge of 10% chord diameter.

separation and, consequently, have undesirable effects on the airfoil performance. These peaks of C_p also occur in the case where the sailwing has a smaller round spar (Fig. 9) or an oval leading edge spar (Fig. 10). The sailwing in Fig. 11 has a leading edge which has the same profile form of NACA6412 within the 7.5% chord from the leading edge, and connects smoothly in the rear half of the leading edge with the membrane. Sweeney et al.[5] call this type of leading edge a "D-spar leading edge." The upper and lower surfaces of the sailwing have 5 and 1% slack respectively. The D-spar leading edge sailwing shows a large improvement in regard to the pressure peaks discussed earlier (Figs. 7-10). Consequently, better performance is expected to be obtained with a D-spar leading edge than with the round spar leading edge. This is in qualitative agreement with the experimental results reported by Fink[7] showing that the D-spar gave a higher L/D value than the round spar, and is confirmed further by the results reported by Sweeney, et al.,[9] showing that the D-spar improved airfoil efficiency compared to the round spar in their windmill experiments.

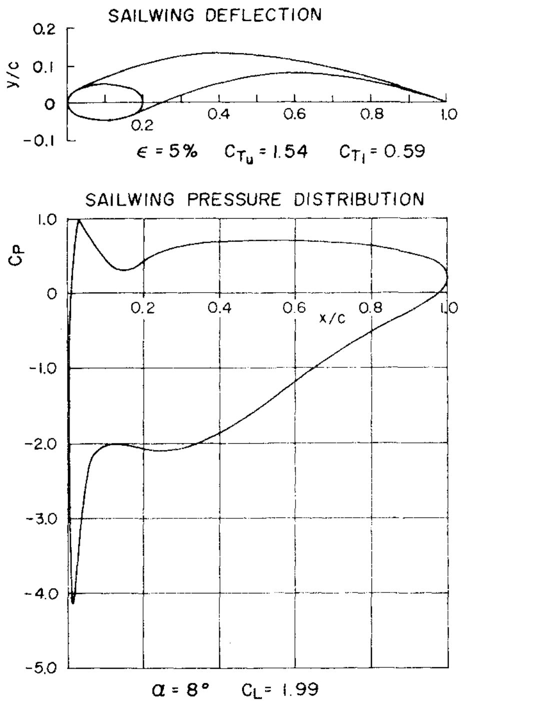

Fig. 10 Sailwing with ellipse leading edge of 20% × 10% chord diameters.

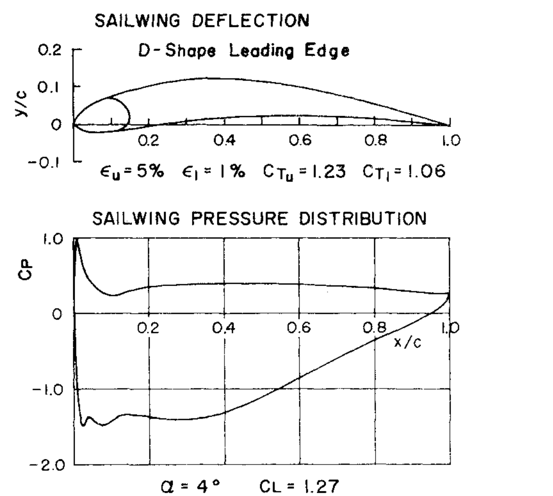

Fig. 11 Removal of pressure peaks by a D-shape leading edge spar and difference of slacknesses between upper and lower surfaces.

Conclusion

A theoretical method has been developed for two-dimensional numerical analysis of the aerodynamic characteristics of a sailwing airfoil with a rounded leading edge and separate upper and lower wing surfaces (membranes) for the conditions that the trailing edge is fixed and the membranes are not stretched by tension. Through numerical examples it is demonstrated that:

1) The pressure distribution on a sailwing with a rounded leading edge is completely different from the one on a single membrane sailwing.

2) A sailwing with a circular or oval type leading edge has sharp suction peaks in the pressure distribution which may have undesirable effects on sailwing performance.

3) A D-spar sailwing with a leading edge of some kind exhibits less pronounced pressure peaks, explaining the improvements of sailwing performance obtained with a D-spar leading edge in the experiments by Sweeney, et al.,[9] and Fink.[7]

References

[1]Thwaites, B., "The Aerodynamic Theory of Sails, I. Two-Dimensional Sails," *Proceedings of Royal Society of London,* Vol. 261, May 1961, pp. 402-422.

[2]Nielsen, J.N., "Theory of Flexible Aerodynamic Surfaces," *Journal of Applied Mechanics,* Vol. 30, *Transactions of ASME, Series E,* Sept. 1963, pp. 435-442.

[3]Tuck, E.O. and Haselgrove, M., "An Extension of Two-Dimensional Sail Theory," *Journal of Ship Research,* Vol. 16, June 1972, pp. 148-152.

[4]Ormiston, R.A., "Theoretical and Experimental Aerodynamics of the Sailwing," *Journal of Aircraft,* Vol. 8, Feb. 1971, pp. 77-84.

[5]Sweeney, T.E., "Exploratory Sailwing Research at Princeton," Princeton University AMS Rept. 578, Dec. 1961.

[6]Fink, M.P., "Full-Scale Investigation of the Aerodynamic Characteristics of a Model Employing a Sailwing Concept," NASA TN D-4062, July 1967.

[7]Fink, M.P., "Full-Scale Investigation of the Aerodynamic Characteristics of a Sailwing of Aspect Ratio 5.9," NASA TN D-5047, Jan. 1969.

[8]Sweeney, T.E. and Nixon, W.B., "An Introduction to the Princeton Sailwing Windmill," Princeton University AMS Rept. 1106, June 1973.

[9]Sweeney, T.E., Nixon, W.B., Maugher, M.D., and Blaha, R., "Sailwing Windmill Characteristics and Related Topics," Princeton University AMS Rept. 1240, 1975.

[10]Ormsbee, A.I. and Chen, A.W., "Multiple Element Airfoils Optimized for Maximum Coefficient," *AIAA Journal,* Vol. 10, Dec. 1972, pp. 1620-1624.

[11]Hess, J.L. and Smith, A.M.O., *Progress in Aeronautical Sciences,* Pergamon Press, New York, 1st Ed., Vol. 8, 1967, pp. 1-39.